Journal of Power Sources, 25 (1989) 141 - 150

OXIDE-BASED BIFUNCTIONAL OXYGEN ELECTRODE FOR RECHARGEABLE METAL/AIR BATTERIES

A. M. KANNAN, A. K. SHUKLA and S. SATHYANARAYANA

Solid State and Structural Chemistry Unit, Department of Inorganic and Physical Chemistry, Indian Institute of Science, Bangalore -560 012 (India)

(Received May 25, 1988; in revised form August 31, 1988)

Summary

Statistical methods for optimizing the morphology of oxide-based, bifunctional oxygen electrodes for use in rechargeable metal/air batteries are examined with regard to binder composition, compaction time, and compaction load. Results show that $LaNiO_3$ with PTFE binder in a nickel mesh envelope provides a satisfactory electrode.

Introduction

Considerable effort has been devoted to understanding and improving the electrocatalytic properties of the oxygen electrode in respect of its use in fuel cells and metal/air batteries [1, 2]. The development of a rechargeable air electrode with high efficiency for batteries has proved to be especially difficult. The most effective electrodes generally require a catalytic coating containing a noble metal such as platinum. This, however, increases costs and attempts have therefore been made to discover alternative, less expensive, catalytic materials. Recently, various transition metal oxides with spinel, perovskite or pyrochlore frameworks have been reported [3 - 11] as promising non-noble metal catalysts both for the oxygen reduction reaction (ORR) and the oxygen evolution reaction (OER).

During recharge of a metal/air battery, oxygen is evolved at the air electrode according to the reaction:

$$4OH^- \longrightarrow O_2 + 2H_2O + 4e^- \quad (1)$$

Undesirable effects have been observed at the potential required for this reaction to proceed at a significant rate, *viz.*, corrosion and/or erosion of the electrode support and the electrocatalyst layer. For this reason, oxygen (or air) electrodes developed for use in fuel cells cannot be employed directly in metal/air batteries; the morphology of the electrode material has to be modified. The proposed use [12] of a third, auxiliary electrode during bat-

0378-7753/89/$3.50

tery recharge has the disadvantage of both lowering the energy density and complicating the operation of the system.

Since the electrode morphology is determined mainly by the binder composition, the compaction load, and the compaction time, and since these factors, in turn, influence each other, it is necessary to conduct a statistical optimization of the electrode fabrication process [13, 14]. Accordingly, a full-factorial design [15 - 17] has been undertaken to optimize the electrode morphology with regard to the above three parameters. The pressure of the feed gas (oxygen) was kept constant at a pre-determined level during the study.

Experimental

Preparation of oxide catalysts

$NiCo_2O_4$, $LaNiO_3$, $LaCoO_3$, $La_{0.1}Sr_{0.9}FeO_3$, and $La_{0.7}Sr_{0.3}MnO_3$ oxide catalysts were synthesized by heating the required stoichiometric proportions of their nitrates at ~900 °C in air. Formation of the oxide catalysts was confirmed by X-ray diffraction analysis using a JEOL powder diffractometer. The average particle size and the specific surface area of the various oxide catalysts were measured with a Cilas–Alcatel-715 granulometer and a Micromeritics-2100 E surface area analyzer, respectively. The average particle size was 16 μm and the average surface area was 5 $m^2 g^{-1}$.

Preparation of electrodes

Preliminary experiments showed that woven nickel-mesh screen (mesh size: 2200 mesh cm^{-2}; wire diameter: 0.07 mm) gave satisfactory service, both as a current collector and as a means of providing mechanical strength to the electrode. Prior to use, the screens were cleaned electrolytically in a concentrated solution of potassium hydroxide. Commercial, battery-grade carbonyl-nickel powder (INCO 255) was mixed ultrasonically with appropriate amounts of each electrocatalyst and a binder (PTFE suspension) to form the active material of the ORR electrode (b, Fig. 1). This mixture was sandwiched between two woven nickel screens (a, c, Fig. 1) under a hydraulic press. The electrodes thus obtained were mechanically rugged and were prepared under different conditions, detailed below in Tables 1 & 2.

The nickel mesh placed on the rear side of the active material, *i.e.*, the gas side (a, Fig. 1) acts as current collector. The mesh facing the electrolyte (c, Fig. 1) provides the site for the OER during anodic polarization of the electrode. With this arrangement, it has been possible to divert the major component of the current to the latter mesh during the anodic OER, and to the hydrophobic catalytic layer (b, Fig. 1) during the cathodic ORR.

Catalytic electrodes with $LaNiO_3$ have also been fabricated without nickel powder in order to compare their performance with those containing nickel powder.

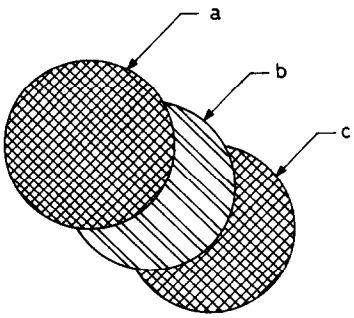

Fig. 1. Configuration of bifunctional oxygen electrode: a, nickel grid to act as the ORR current-collector; b, hydrophobic layer made from oxide catalyst, PTFE binder, and (in some cases) nickel powder (INCO 255) conducting matrix for the ORR; c, nickel grid for the OER.

TABLE 1

Values of various individual parameters at two levels

Parameters	Value of variable	
	(—) Low level	(+) High level
A Teflon composition (wt.%)	10	30
B Compaction pressure (kg cm^{-2})	40	240
C Compaction time (s)	60	300

TABLE 2

Test matrix for 2^3-factorial design

Run no.	Various treatment combinations*	Parameters		
		A	B	C
1	L	—	—	—
2	a	+	—	—
3	b	—	+	—
4	ab	+	+	—
5	c	—	—	+
6	ac	+	—	+
7	bc	—	+	+
8	abc	+	+	+

*L, All three parameters A, B and C at low levels.
a, Parameter A at high level; others at low levels.
ab, Parameters A and B at high levels; C at low level.
abc, Parameters A, B and C at high levels.
Similarly for other combinations.

Electrochemical characterization of electrodes

A diagram of the cell employed for electrochemical characterization is shown in Fig. 2. The cell comprised a rectangular plexiglas container with a lid that held a reference electrode, a counter electrode, a heating element coupled to a temperature controller, and a thermometer. The cell temperature was maintained at 30 °C. The oxygen electrode was located on one of the walls of the container and was supplied with oxygen from the rear. The electrolyte consisted of 6 M KOH and was stirred throughout the experiment. The potential of the working electrode was recorded against an Hg/HgO, KOH (6 M) reference electrode during both the ORR and the OER. All potentials are reported with regard to this electrode. Steady-state current/potential curves were obtained galvanostatically using a sintered-nickel-plaque counter electrode.

Statistical method

Prior to statistical optimization, several polarization studies were conducted to evaluate the catalytic activity of various electrocatalysts, both for the ORR and the OER. These experiments indicated that $LaNiO_3$ is the best electrocatalyst since this material exhibited the lowest polarization at all current densities up to 30 mA cm^{-2}. As mentioned earlier, the main parameters that determine electrode performance are: PTFE composition (A); compaction load (B); compaction time (C). Since these parameters also influence each other, a statistical optimization has been carried out following the procedure given in ref. 14. The limits of these parameters and the design matrix of the experiments adopted for the optimization are listed in Tables 1 and 2, respectively. The parameters influence the polarization behaviour of the electrode, which can be mathematically expressed as:

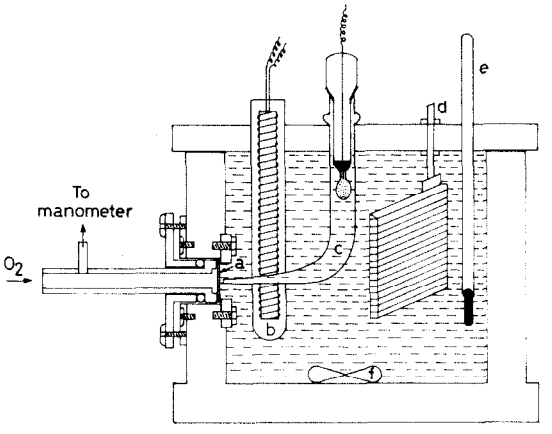

Fig. 2. Electrochemical cell assembly: a, working electrode; b, heating element; c, Luggin capillary; d, counter electrode; e, thermometer; f, magnetic stirrer (pellet).

$$Y = f(x_1, x_2, x_3, \ldots x_n) \tag{2}$$

where the x_i series represents the input parameters. To simplify the analysis, normalized parameters x_i^* are defined for a two-level system:

$$x_i^* = (x_i - [x_i(+) + x_i(-)]/2)/([x_i(+) - x_i(-)]/2) \tag{3}$$

where $x_i(+)$ and $x_i(-)$ are the upper and lower limits of parameter x_i and optimization is most effectively performed within these limits. It is evident that x_i^* will take the value +1 when $x_i = x_i(+)$ and −1 when $x_i = x_i(-)$. If a polynomial relationship exists between Y and the x_i parameters, or equivalently the x_i^*, then eqn. (2) may be written in the form:

$$Y = m_0 + \sum_i m_i x_i^* + \sum_i \sum_{i<j} m_{ij} x_i^* x_j^* + \ldots + m_{123 \ldots n} x_1^* x_2^* \ldots x_n^* \tag{4}$$

where the m factors, m_1, $m_2 \ldots m_n$, in eqn. (4) describe the effect of the individual parameters and $m_{ij}, \ldots m_{ijk}, \ldots$ represent the effect of the coupled action of the parameters. In this scheme, an optimum is found for the various input parameters under the assumption that respective changes are linear.

In the present study, the levels fixed for the three parameters (*i.e.*, A - C) to be optimized and their eight combinations (L - abc) are given in Tables 1 and 2, respectively. The full 2^3-factorial design* required eight trial runs: one average effect; three main effects; three first order effects; one second order effect.

Results and discussion

The results of various trials, together with Yates' analysis* of the data both for the ORR and the OER when using $LaNiO_3$ as electrocatalyst, are given in Tables 3 and 4, respectively. The first step is to arrange the electrode potentials in the standard order, *i.e.*, as in column 2 of Tables 3 and 4, and then to derive, in turn, columns 3, 4, 5 and 6. The first four values in each column 3 are calculated by summing successive pairs of values in the corresponding column 2. The remaining four values in column 3 are obtained by taking the difference between the sucessive pairs in column 2. The data in columns 4 and 5 are determined in a similar fashion from pairs of values in the preceding column. The mean-difference values given in column 6 of Tables 3 and 4 indicate the relative effects of each parameter and their interactions. In order to obtain optimum electrode performance, a parameter must be shifted from its average value to a higher value for a positive effect and to a lower value for a negative effect, as dictated by Yates' analysis [15].

*The full 2^3-factorial design for statistical optimization, as well as Yates' analysis of such experimental data, are explained in detail in ref. 15.

TABLE 3

2^3-factorial design for the oxygen reduction reaction (ORR)

Treatment combinations	Potential at 20 mA cm^{-2} (V)	Yates' analysis [15]				
		I	II	III	Mean difference III/4	Total effect
L	−0.055	−0.297	−0.364	−0.702	−0.1755	Grand Total
a	−0.242	−0.067	−0.338	−0.376	−0.094	A
b	−0.037	−0.280	−0.180	0.452	0.113	B
ab	−0.030	−0.058	−0.196	0.418	0.1045	AB
c	−0.035	−0.187	0.230	0.026	0.0065	C
ac	−0.245	0.007	0.222	−0.016	−0.004	AC
bc	−0.036	−0.210	0.194	−0.008	−0.002	BC
abc	−0.022	0.014	0.224	0.030	0.0075	ABC

TABLE 4

2^3-factorial design for oxygen evolution reaction (OER)

Treatment combinations	Potential at 100 mA cm^{-2} (V)	Yates' analysis [15]				
		I	II	III	Mean difference III/4	Total effect
L	0.632	1.297	2.565	5.089	1.272	Grand Total
a	0.665	1.268	2.524	0.057	0.014	A
b	0.618	1.283	0.065	−0.071	−0.018	B
ab	0.650	1.241	−0.008	−0.043	−0.011	AB
c	0.633	0.033	−0.029	−0.041	−0.010	C
ac	0.650	0.032	−0.042	−0.073	−0.018	AC
bc	0.633	0.017	−0.001	−0.013	−0.003	BC
abc	0.608	−0.025	−0.042	−0.041	−0.010	ABC

Assuming the reversible potential (E_r) of the oxygen electrode to be 0.3 V, the data in column 6 of Tables 3 and 4 show that the effect of parameters A and B on polarization (see mean difference column) is significant in the case of the ORR (Table 3), but is negligible for the OER (Table 4). Final experiments were designed, therefore, to investigate the relative effects of the parameters on the ORR alone. These are summarized in Table 5. The polarization performance of the optimized electrode for both the ORR and the OER is given in Fig. 3 (in addition to Table 5). The performance curve for an $LaNiO_3$ bifunctional oxygen electrode [3] is also shown in Fig. 3.

The electrochemical polarization data of the present work have not been compensated for *iR*-losses. The actual performance (*iR*-free polarization) will therefore be superior to that reported here.

TABLE 5

Final design of the electrodes from Table 3

No.	A (wt.%)	B (kg cm^{-2})	C (s)	ORR potential at 30 mA cm^{-2} (V)	OER potential at 100 mA cm^{-2} (V)
9	18.3	160	200	−0.033	0.620
10	16.6	180	225	−0.019	0.600
11	15.0	200	250	−0.043	0.605

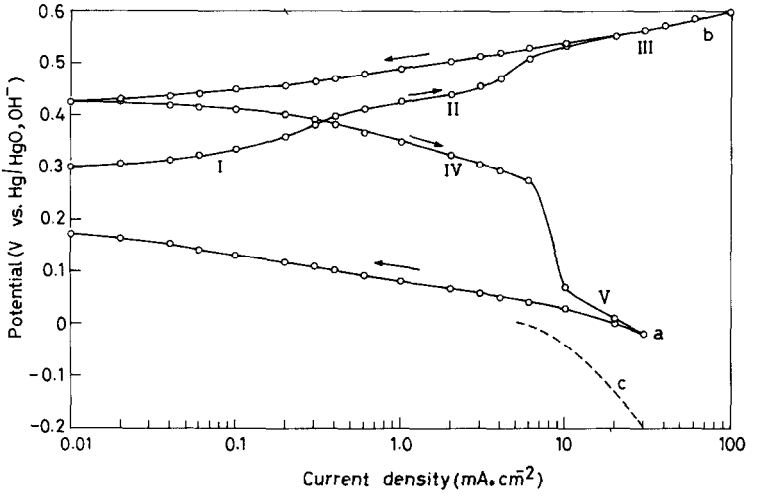

Fig. 3. Polarization curves at 30 °C in 6 M KOH for: a, ORR; b, OER on $LaNiO_3$-based bifunctional oxygen electrode containing 30% Ni powder; c, ORR on $LaNiO_3$ bifunctional oxygen electrode from ref. 3. Arrows indicate direction of scan.

The anodic polarization curves (b, Figs. 3 and 4) exhibit hysteresis when the current is changed from a low to a high value and then reversed to a low value. Step I in Fig. 3, lying between 0.3 V and 0.4 V is probably due to the simultaneous onset of the following reactions:

(i) oxidation of perhydroxyl ion formed during the ORR, *i.e.*,

$OH^- + HO_2^- \longrightarrow O_2 + H_2O + 2e^-$ ($E_r = -0.08$ V assuming $[HO_2^-] \approx 10^{-3}$ M);

(ii) oxidation of Ni^{2+} to Ni^{3+}, *i.e.*,

$Ni(OH)_2 + OH^- \longrightarrow NiOOH + H_2O + e^-$ ($E_r = 0.39$ V);

(iii) oxygen evolution (OER), *i.e.*,

$4OH^- \longrightarrow O_2 + 2H_2O + 4e^-$ ($E_r = 0.30$ V).

The peroxide concentration of about 10^{-3} M is low [18], as confirmed by a low limiting-current value of ~ 0.2 mA cm^{-2} for step I.

Step II in Fig. 3, between 0.4 V and 0.5 V may be due to: (i) oxidation of Ni^{2+} to Ni^{3+} through a proton-transfer process; (ii) evolution of oxygen. After oxidation of Ni^{2+} to Ni^{3+} is complete, the potential rises above 0.55 V (step III, Fig. 3) and steady evolution of oxygen occurs. As is evident from Fig. 3, b, the OER only takes place when the current is reversed from a high to a low value.

Subsequent to anodic polarization, when the electrode is polarized cathodically, a plateau (step IV, Fig. 3, a), corresponding to the reduction of β-NiOOH to $Ni(OH)_2$ is observed between ~ 0.4 V and 0.3 V. There follows a drop in potential from 0.3 V to 0.05 V at ~ 6 mA cm^{-2}. This behaviour can be attributed to the polarization necessary to sustain the ORR at the electrode. The polarization curve then follows the usual ORR curve (step V). The oxide layer of β-NiOOH formed during the anodic polarization of the electrode is unstable; the electrode potential after anodic polarization up to 0.61 V returns to a value of 0.42 V (step II, Fig. 3, a) soon after opening the circuit, and finally approaches the potential of step I after ~ 24 h. These observations are in agreement with those reported by Hoare [19].

The performance of $LaNiO_3$ electrodes compacted under optimum conditions *without* nickel powder was found to be very similar to those containing nickel (see Fig. 4). This finding is probably associated with the fact that $LaNiO_3$ is itself a good electrical conductor; it has a conductivity of 100 ohm^{-1} cm^{-1} at room temperature [20] and, hence, behaves as a "metal".

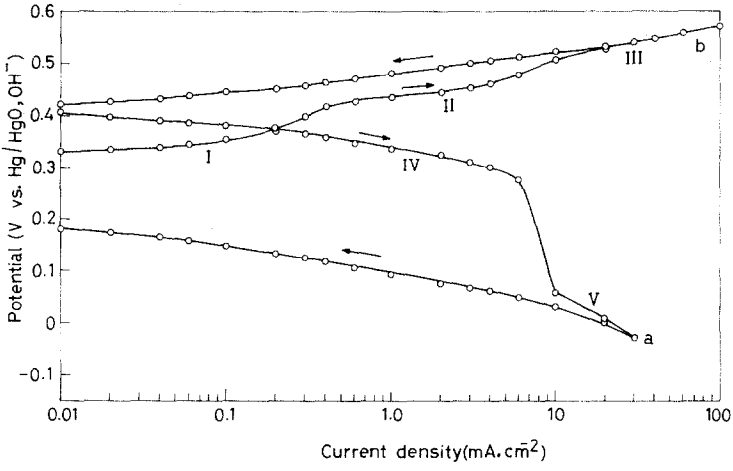

Fig. 4. Polarization curves at 30 °C in 6 M KOH for: a, ORR; b, OER. $LaNiO_3$-based bifunctional oxygen electrode without nickel power. Arrows indicate direction of scan.

The rest potentials of all the electrodes deviated significantly from the E_r value of the oxygen electrode (*i.e.*, 0.3 V). This is to be expected because the electrochemical splitting of the oxygen molecule is strongly impeded by the high stability of the O=O double bond. Hydrogen peroxide (H_2O_2) is formed as an intermediate product and gives rise to a mixed potential; this is an inherent feature of any oxygen electrode.

Conclusions

Oxide-based materials have been tested as electrodes for both oxygen evolution (OER) and oxygen reduction (ORR) at 30 °C. Electrodes containing $LaNiO_3$ show the best catalytic activity. The electrodes can withstand a load current density of 30 mA cm^{-2} with a polarization of <0.2 V from the rest potential in the cathodic mode (ORR) and 100 mA cm^{-2} with a polarization of ~ 0.2 V in the anodic mode (OER). It is noteworthy that the performance characteristics of the $LaNiO_3$-based bifunctional oxygen electrodes fabricated without statistical optimization have recently been reported [3] to show a polarization as high as ~ 0.3 V at 30 mA cm^{-2} during cathodic operation. This performance is inferior to that of electrodes reported in this study and demonstrates the benefits of adopting a statistical optimization procedure. In addition, electrodes obtained using the statistical optimization method are mechanically rugged and do not disintegrate during charge/discharge operations.

Acknowledgement

The authors are grateful to the Department of Non-conventional Energy Sources, Ministry of Energy, Government of India, New Delhi, for providing financial support for this work.

References

1 H. Tamura, H. Yoneyama and Y. Matsumoto, in E. Trasatti (ed.), *Electrodes of Conductive Metallic Oxides, Part-A*, Elsevier, Amsterdam, 1980, p. 261 and references cited therein.
2 J.O' M. Bockris and T. Otagava, *J. Phys. Chem., 87* (1983) 2960.
3 S. Viswanathan and A. Charkey, *SAE Tech. Pap. No. 859053*, 1985, p. 2.21.
4 A. Wattiaux, J. C. Grenier, M. Pouchard and P. Hagenmuller, *J. Electrochem. Soc., 134* (1987) 1714.
5 P. N. Ross, *Proc. 21st Intersoc. Energy Conv. Eng. Conf., 1986*, p. 1066.
6 J. Haenen, W. Visscher and E. Barendrecht, *J. Electroanal. Chem., 208* (1986) 273.
7 H. S. Horowitz, J. M. Longo and H. H. Horowitz, *J. Electrochem. Soc., 130* (1983) 1851.
8 J. A. R. Van Veen, J. M. Van Der Eijk, R. De Ruiter and S. Huizinga, *Electrochim. Acta, 33* (1983) 1851.

9 R. E. Carbonio, C. Fierro, D. Tryk, D. Scherson and E. Yeager, *NASA Conf. Publ. 2484*, 1987, p. 221.
10 L. Swette and J. Giner, *NASA Conf. Publ. 2484*, 1987, p. 237.
11 D. O. Ham, G. Moniz and E. J. Taylor, *NASA Conf. Publ. 2484*, 1987, p. 245.
12 S. Hattori, M. Yamura, C. Kawamura and S. Yoshida, in D. H. Collins (ed.), *Power Sources 4*, Oriel Press, Newcastle upon Tyne, 1973, p. 361.
13 A. M. Kannan, A. K. Shukla and A. Hamnett, *J. Appl. Electrochem., 18* (1988) 149.
14 K. Vijayamohanan, A. K. Shukla and S. Sathyanarayana, *Indian J. Technol., 24* (1986) 430.
15 W. E. Duckworth, *Statistical Techniques in Technological Research*, Methuen and Co., London, 1968.
16 G. E. P. Box, W. G. Hunter and J. S. Hunter, *Statistics for Experimenters*, Wiley, New York, 1978.
17 N. L. Johnson and F. C. Leone, *Statistics and Experimental Design in Engineering and Physical Sciences*, Vol. 2, Wiley, New York, 1977.
18 W. G. Berl, *Trans. Electrochem. Soc., 82* (1943) 253.
19 J. P. Hoare, *Electrochemistry of Oxygen*, Wiley, New York, 1968.
20 H. Obayashi and T. Kudo, *J. Appl. Phys. Jpn., 14* (1975) 330.